PB80-219470

Study of Deep Mining Operational Economics Volume I. Simulation Development and Study of Obstacle Effects

Science Applications, Inc.
La Jolla, CA

Prepared for

Bureau of Mines
Washington, DC

Sep 79

U.S. Department of Commerce
National Technical Information Service
NTIS

PB80-219470

BuMines OFR 95(1)-80

STUDY OF DEEP OCEAN MINING

OPERATIONAL ECONOMICS

Vol. I. Simulation Development and Study of Obstacle Effects

Submitted

September 1979

by

David R. Peterson
and
Philip B. Grote

This report was prepared in response
to the U.S. Department of Interior
under Bureau of Mines Contract J0177131

Bureau of Mines Open File Report 95(1)-80

REPRODUCED BY
NATIONAL TECHNICAL
INFORMATION SERVICE
U.S. DEPARTMENT OF COMMERCE
SPRINGFIELD, VA 22161

50272-101

REPORT DOCUMENTATION PAGE	1. REPORT NO. BuMines OFR 95(1)-80	2.	3. Recipient's Accession No. PB80 219470
4. Title and Subtitle Study of Eeep Ocean Mining Operational Economics. Vol. I. Simulation Development and Study of Obstacle Effects			5. Report Date September 1979 6.
7. Author(s) David R. Peterson and Philip B. Grote			8. Performing Organization Rept. No.
9. Performing Organization Name and Address Science Applications, Inc. P.O. Box 2351 La Jolla, CA 92037			10. Project/Task/Work Unit No. 11. Contract(C) or Grant(G) No. (C) J0177131 (G)
12. Sponsoring Organization Name and Address Office of the Director--Minerals Health and Safety Technology Bureau of Mines U.S. Department of the Interior Washington, DC 20241			13. Type of Report & Period Covered Contract research 14.

15. Supplementary Notes

Approved by the Director, Bureau of Mines, for placement on open file, July 31, 1980.

16. Abstract (Limit: 200 words)

This report presents a deep ocean mining operational simulation that is capable of describing the response of the bottom collection unit to specified mining ship maneuvers and the corresponding operation of the mining ship maneuvering system. Bathymetry, obstacles, collector and pipe dynamics, and ship maneuvering capabilities are included in the simulation. The simulation is capable of evaluating the technical requirements and operating costs for specified mine plans. Results are useful in assessing mine size requirements and provide operating cost estimates useful as inputs to deep ocean mining economic feasibility assessments. The simulation is used to determine the consequence of obstacles to mining system operations in terms of impact on mine size requirements and reduced production arising from obstacle avoidance maneuvers of a towed (unsteered) collector.

17. Document Analysis a. Descriptors

Deep ocean mining
Nodule mining
Dynamic simulation
Operational simulation

b. Identifiers/Open-Ended Terms

c. COSATI Field/Group 08I

18. Availability Statement	19. Security Class (This Report)	21. No. of Pages
Unlimited release by NTIS.	20. Security Class (This Page)	22. Price

(See ANSI-Z39.18) See Instructions on Reverse OPTIONAL FORM 272 (4-77) (Formerly NTIS-35) Department of Commerce

DISCLAIMER NOTICE

The views and conclucions contained in this document are those of the authors and should not be interpreted as necessarily representing the official policies or recommendations of the Interior Department's Bureau of Mines or of the U.S. Government.

FOREWORD

This report was prepared by Science Aplications, Inc., Offshore Technology Division, P.O. Box 2351, 1200 Prospect Street, La Jolla, California 92037, under USBM Contract Number J0177131. The contract was initiated under the Branch of Foreign Data. It was administered under the technical direction of TCMRC with Dr. Robert Willard acting as the Technical Project Officer. Mr. Howard Eveland was the contract administrator for the Bureau of Mines.

This report summarizes the work completed as part of this contract. Volume 1 is the Final Report. Volume 2 is a User's Manual.

TABLE OF CONTENTS

Section		Page
	Executive Summary	iv
1.	Introduction	1
2.	Simulation Approach	2
3.	Definition of Terms	5
4.	Demonstration Cases	7
5.	Study of Operations with Respect to Obstacles	13
6.	Effects of Obstacles on Mine Development and Requirements	19
7.	Formulation of the DOMOPS Capability	22
8.	Conclusions and Recommendations	37
9.	References	39
Appendix A.	Nomenclature	A-1
Appendix B.	Development of a Simple Model for Lift Pipe Behavior	B-1

Executive Summary

This report describes a deep ocean mining operational simulation (DOMOPS) which has been recently completed under a U.S. Bureau of Mines contract. A major consideration in the development of the simulation has been to provide a tool which could address the many diverse mining system operational issues without incurring large computational costs.

The first part of the paper presents a simplified methodology for simulating the maneuvers of a deep ocean mining system on a nodule mine site. The following are represented in the simulation: bathymetry, obstacles, collector dynamics, pipe dynamics, mining ship maneuvers, and prevailing weather patterns. The simulation predicts the collector path and areal efficiency in response to mine ship maneuvers and the associated fuel costs.

In the second part of the paper, a methodology for quantifying the effects of obstacles in terms of mine area requirements, production rate, and operating cost is developed and illustrative examples are presented.

Figure 2.1 shows the basic logic of the DOMOPS simulation, and the detailed formulation of equations is presented in Section 7 and Appendix B. Essentially the simulation consists of two major components or modules. One simulates the trajectory of the mining ship in response to maneuvering system commands for a given weather condition. The second simulates the interaction between the mining ship and collector through the lift pipe and the collector response to the topography of the ocean bottom.

The mining ship maneuvering system includes the ship main propulsion system, rudder, and bow and stern thrusters. Maneuvering system characteristics include specified operating constraints, such as maximum rudder force, rudder maximum response rate, maximum horsepower available, maximum horsepower rate of change, maximum propulsion system torque, maximum propulsion system RPM, and constraints on maneuvers dictated by motions of the pipe in the mine ship moonpool.

The collector maneuvering simulation simulates the trajectory of a passively towed collector on a deterministic bathymetric map in response to the mining ship trajectory. The topography as described by a bathymetric map and the ship trajectory represent inputs to the collector system. Figures 4.3 and 4.4, as examples, demonstrate the effects of rough terrain on the collector path performance.

Figure 5.1 illustrates a basic strategy for obstacle avoidance. In a region around the obstacle, successive collector swaths are compressed together and a turning maneuver is required to avoid the obstacle. In reality, the collector trajectories resulting from an obstacle avoidance maneuver will not be smooth paths as illustrated in Figure 5.1, but will be subject to random lateral motion due to the effects of rough terrain. Figure 5.4 illustrates a realization of a maneuver on a random topography around a 400 foot (length)) obstacle.

These initial investigations were based upon utilization of the DOMOPS capability. The DOMOPS program is an efficient tool (23 cents per mile) for analyzing deep ocean mining operations, including:

- Obstacles
- Rough terrain
- Weather
- Mining system design parameters
- Operational parameters

In addition, several general conclusions can be stated:

- Rough terrain decreases both sweep efficiency and feed efficiency of nodule collection

- Collector maneuverability from the surface is greatly limited by the length of the lift pipe and the drag of seawater

- Increasing forward velocity of the collector increases sensitivity to side slopes

- Lift pipe drag has a significant effect on mining ship maneuverability

The presence of obstacles further reduces sweep efficiency and feed efficiency. However, this reduction is minimal for a system whose sweep efficiency is low to begin with. Other conclusions regarding obstacle effects are as follows:

- The effect of an obstacle may be viewed as occurring over an obstacle affected area in which feed and sweep efficiency are modified. The overall effects on the mine site are thus obtained by combining the sweep efficiency and feed efficiency for obstacle and nonobstacle areas on an area weighted basis.

- Effects of obstacles are sensitive to the controllability of the collector. The results presented account for the effects of rough terrain. Other effects such as navigational error, wave drift forces, temporal and spatial current variations will further degrade performance with respect to obstacles and in general. However, these effects can be countered by using collector steering.

- Using the same miss distance for all obstacle paths minimizes obstacle avoidance operating cost, cost of lost production, and also maximizes mine site recovery rate.

- Overall assessment of obstacle effects on mine area, recovery rate, and average production rate requires utilization of information on obstacle size distribution and spatial density.

1. INTRODUCTION

The capability of an ocean miner to maneuver on a mine site, and the cost of these maneuvers, is a major consideration in the development of operational plans. Such plans may be viewed as including a specification of the trajectories of the mining ship and the interconnected collector so that an acceptable ore recovery rate can be achieved at minimum operating cost. Because of the multiplicity of potential mine plans that could be envisaged for a given mine area, a low-cost maneuvering simulation capability is desirable to assist in the selection and definition of the plan approach. The objective of the development of the deep ocean mining operational simulation (DOMOPS) was a low-cost capability for simulating these system maneuvers.

Collector maneuverability is an important factor in assessing mining system operations in a number of respects: (1) collector maneuverability determines how well the collector can operate on successive paths to reduce overlap with previous paths. Overlap reduces system production rate and is the factor which limits the sweep efficiency which can be practically achieved in a mine site, and (2) collector maneuverability is important in any assessment of the area effected in the vicinity of an obstacle which is associated with obstacle avoidance maneuvers. Both of these aspects are important in determining mine area requirements and production rate estimates.

The DOMOPS program as described in the following section does not as yet include collector steering. Although collectors will generally be designed to be steered, they may sometimes be operated in a passive mode, for example, when the steering system fails. Therefore, this initial simulation considers only an unsteered collector.

2. SIMULATION APPROACH

This report describes a deep ocean mining operational simulation (DOMOPS) which has been recently completed under a U.S. Bureau of Mines contract. A major consideration in the development of the simulation has been to provide a tool which could address the many diverse mining system operational issues without incurring large computational costs. The authors estimate that the cost of operation of DOMOPS is approximately 23 cents per mile of simulated operation.

Figure 2.1 shows the basic logic of the DOMOPS simulation, and the detailed formulation of equations is presented in Section 7 and Appendix B. Essentially the simulation consists of two major components or modules. One simulates the trajectory of the mining ship in response to maneuvering system commands for a given weather condition. The second simulates the interaction between the mining ship and collector through the lift pipe and the collector response to the topography of the ocean bottom.

The mining ship maneuvering system includes the ship main propulsion system, rudder, and bow and stern thrusters. Maneuvering system characteristics include specified operating constraints, such as maximum rudder force, rudder maximum response rate, maximum horsepower available, maximum horsepower rate of change, maximum propulsion system torque, maximum propulsion system RPM, and constraints on maneuvers dictated by motions of the pipe in the mine ship moonpool.

The collector maneuvering simulation simulates the trajectory of a passively towed collector on a deterministic bathymetric map in response to the mining ship trajectory. The topography as described by a bathymetric map and the ship trajectory represent inputs to the collector system.

Because of the massiveness of the mining ship, the ship's trajectory represents a very low frequency input to the mining system. The simulation takes advantage of this fact by very simply representing the lift pipe. This simplification provides a low-cost but comprehensive simulation capability. The detailed formulation of the equations of motion are presented in Section 7. The primary emphasis in Sections 4, 5, and 6 is on the simulation results and their implications.

Figure 2.2 shows the ship and collector in the global (X,Y,Z) and coordinate system. The location of the collector is (X_C,Y_C,Z_C), and that of the ship center of gravity (CG) is (X_S,Y_S,Z_S).

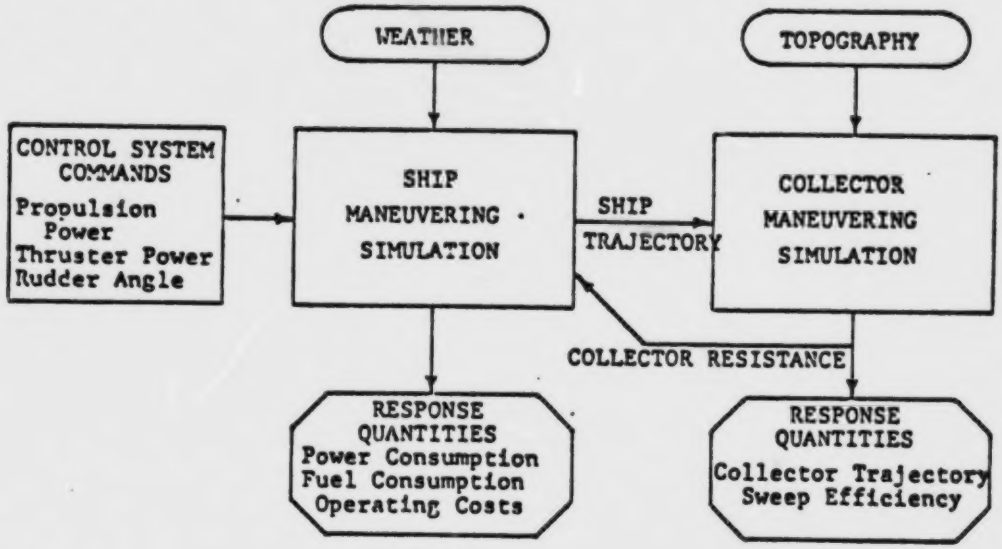

Figure 2.1. Simulation Logic/Capabilities

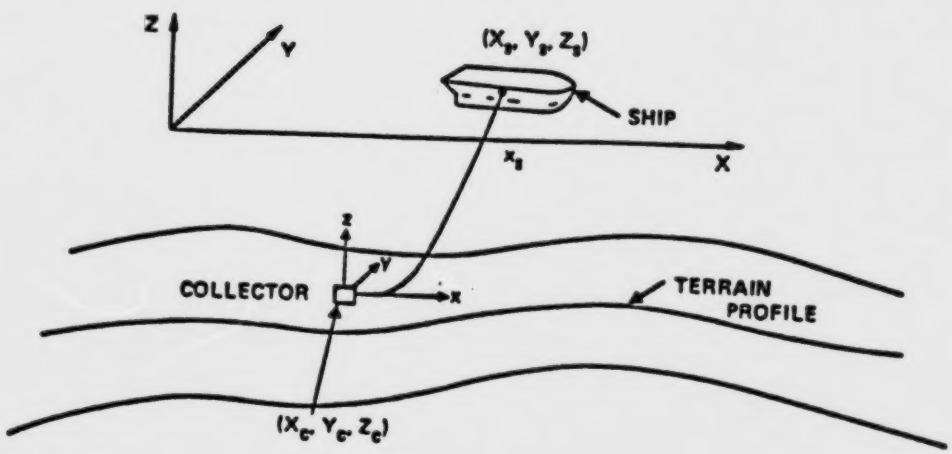

Figure 2.2. Ship/Collector Coordinate Systems

3. DEFINITION OF TERMS

The parameters which are the significant measures of the performance of a deep ocean mining system are:

- Dredge efficiency, η_d
- Sweep efficiency, η_s
- Feed efficiency, η_f
- Recovery rate, R

The dredge efficiency which is dependent on operating speed and probably also nodule concentration, is the percentage of nodules by weight within the swath, S, which are delivered to the surface mining vessel. Thus, dredge efficiency implicitly accounts for: nodules not collected because of burial by the collector running gear (swath efficiency), nodules which the collection device fails to collect (pick-up efficiency), nodule material expelled with excess water from the collector, and nodule material lost at the surface in the process of dewatering.

As mining proceeds in a nodule mine site, the current collector swath tends to overlap with previously mined areas, as indicated by area A_o in Figure 3.1. The two key parameters which measure this effect are feed efficiency and sweep efficiency as illustrated in the figure. Feed efficiency is a measure of the loss of production associated with the overlap, and sweep efficiency is a measure of the mine area consumed in relation to the total mine area. Recovery rate is also defined in the figure, and it is a measure of the percentage of the total ore in the site which is recovered.

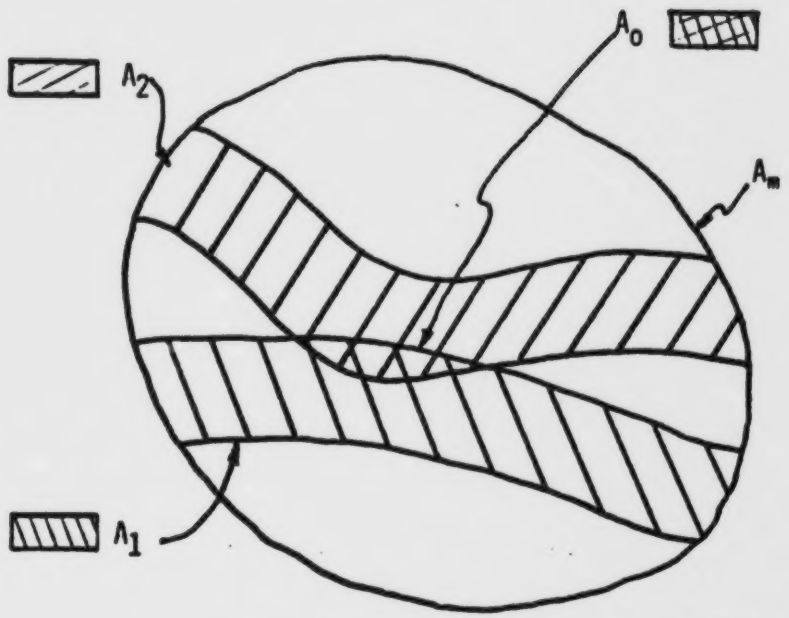

A_m = MINE AREA

A_1 = AREA OF PATH 1

A_2 = AREA OF PATH 2

A_0 = OVERLAP AREA

SWEEP EFFICIENCY, $\eta_s = \dfrac{A_1 + A_2 - A_0}{A_m}$

RECOVERY RATE $R = \eta_d \eta_s$

FEED EFFICIENCY, $\eta_f = \dfrac{A_1 + A_2 - A_0}{A_1 + A_2}$

Figure 3.1. Definition of Sweep Efficiency, Feed Efficiency, and Recovery Rate

4. DEMONSTRATION CASES

It will be useful to present a number of demonstration cases to provide insight into the maneuvering characteristics of a deep ocean mining system and the implication of these to broader deep ocean mining issues. These cases are generally based on the baseline 3 million dry short ton per year (DSTPY) configuration shown in Table 4.1.

System Maneuverability

Figure 4.1 illustrates the effect of the lift string drag on ship maneuverability in a turn when the string is attached at the ship CG. In this case, the string tends to stabilize the ship in the turn. However, if the string is attached further forward a shorter turn radius is feasible, because that reduces the stabilizing effect of the lift string.

Mining in a Trough

Figure 4.2 shows the simulated behavior of the collector in a trough. On successive swaths the collector tends to slide to the bottom of the trough and remine it. This may happen whether coulomb or viscous sediment friction is assumed because in either case the effective lateral friction is viscous.

Rough Terrain

Swath overlap and the associated loss in feed efficiency generally arises from collector control error. Many factors can contribute to collector control error including rough terrain, navigational error, currents, and collector steering limitations. Here we examine only the effect of rough terrain. Hence, the quantitative results represent an optimistic projection of performance. The effects of other sources of collector control error are qualitatively similar, however.

Table 4.1. Base Line Configuration

1. SYSTEM

   A. SHIP

      - Length, 550 ft
      - Beam, 90 ft
      - Draft, 30 ft
      - Displacement, 38,000 tons

   B. LIFT STRING

      - Length, 15,550 ft

   C. COLLECTOR

      - Dredge Efficiency, .6
      - Swath Width, 50 ft
      - Coulomb Friction, μ, .3
      - Weight
      - Mass, Sway
      - Mass, Surge

2. OPERATION

   - Production, 3 M DSTPY
   - Tow Velocity, 5 fps
   - Swath Spacing, 50 ft
   - Nominal Feed Efficiency, .9

3. ENVIRONMENT

   - Calm Seas
   - No Current
   - Nodule Abundance, 2 lb/ft^2

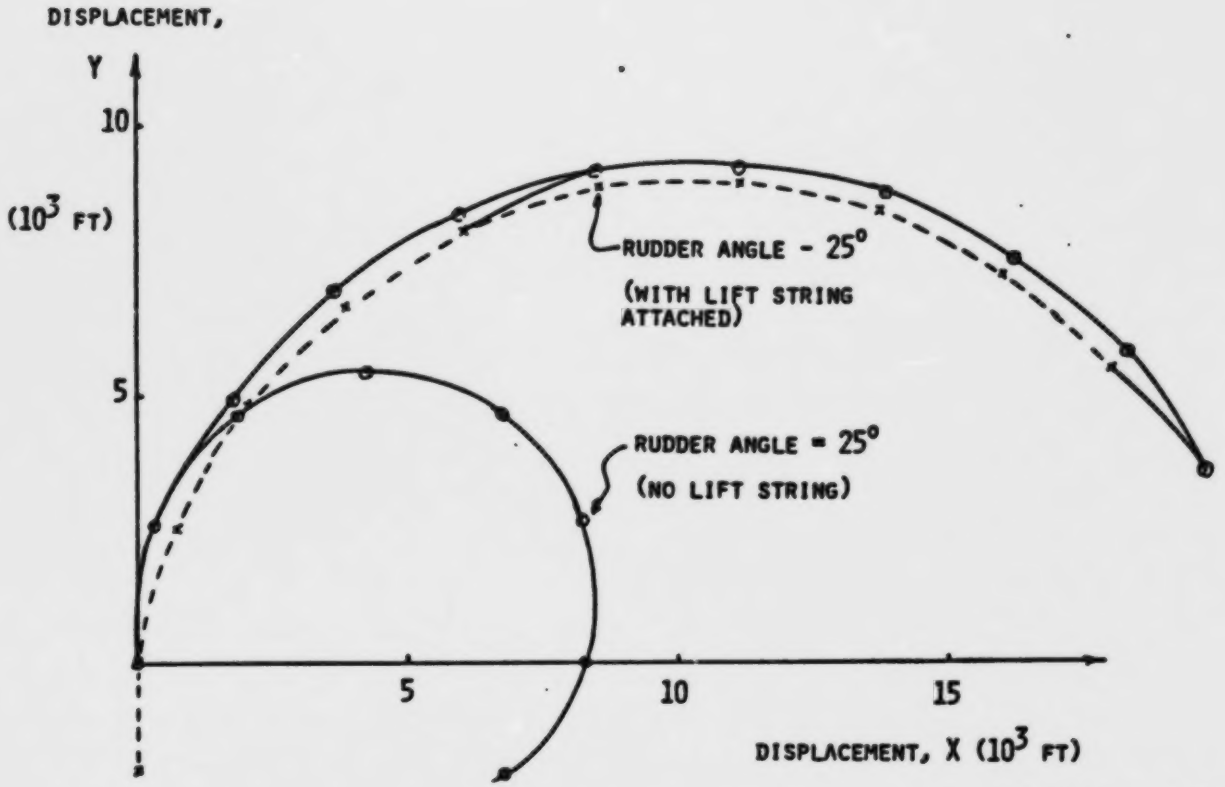

Figure 4.1. Effect of Lift String on Ship Maneuverability During 25° Starboard Turn

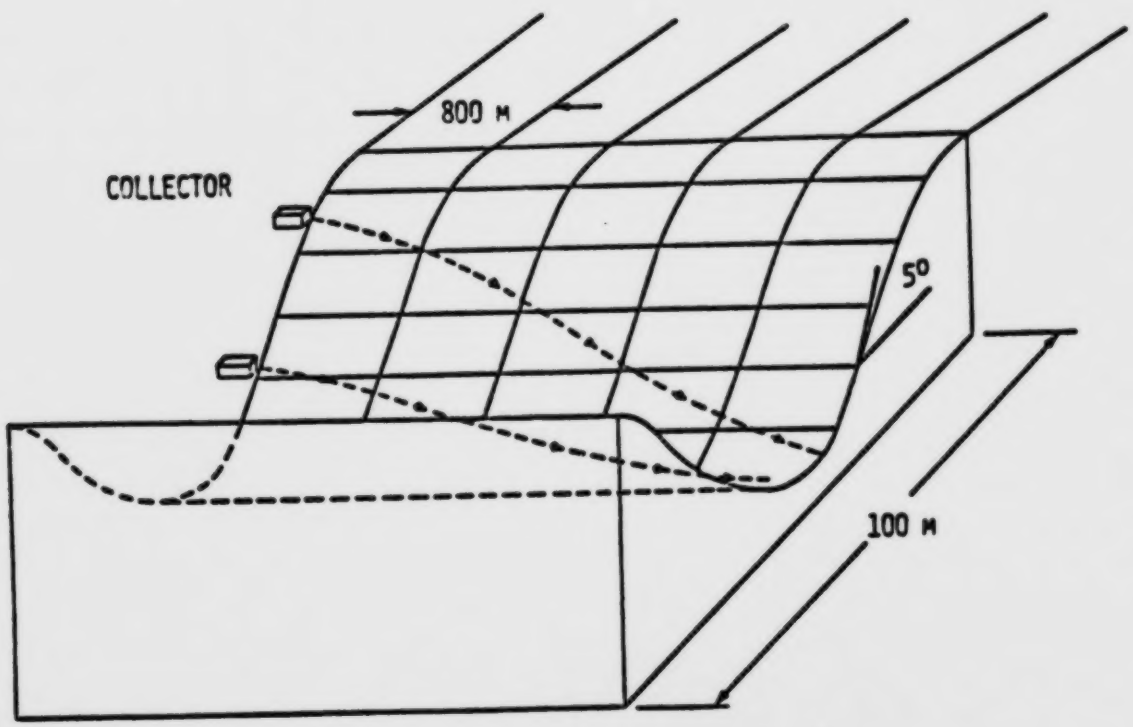

Figure 4.2. Collector Behavior in a Trough

The results in Figures 4.3 and 4.4 were developed by simulating the towing of a collector with a 20 ft swath width on nominally parallel paths spaced a distance d apart. The terrain used was a two dimensional Fourier series realization of terrain described in terms of a power spectral density.

Figure 4.3 shows an inverse relationship between sweep efficiency and feed efficiency. Thus, as one attempts to increase sweep efficiency, feed efficiency falls. As the swath spacing, d, approaches five times the swath width, or 100 ft, the feed efficiency approaches 100 percent. If an average feed efficiency $\eta_f = .9$ is required, as indicated in Table 4.1, to achieve the design production rate, then the swath spacing for the system and terrain assumed should be 60 ft. This results in a sweep efficiency of .3, and using $\eta_d = .6$ from Table 4.1, a recovery rate of 18 percent is achieved.

As swath spacing is decreased, the feed efficiency decreases. Consequently, the production rate decreases. Operating costs remain essentially constant; thus, the cost of production per ton increases as shown in Figure 4.4. The cost of production may also be considered in terms of recovery rate. For this example, Figure 4.5 shows that the operating cost/ton increases rapidly as one attempts to raise recovery rate above 20 percent.

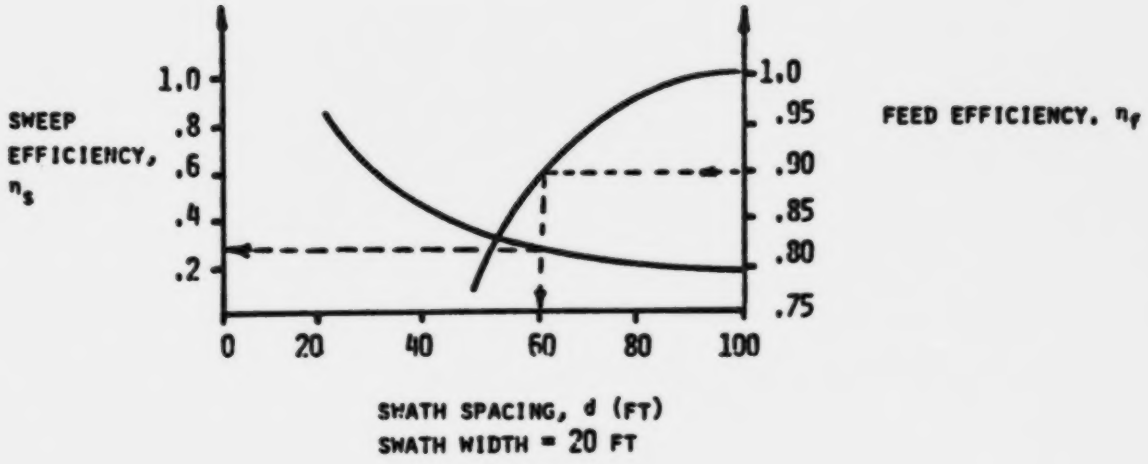

Figure 4.3. Effect of Rough Terrain on Collector Performance

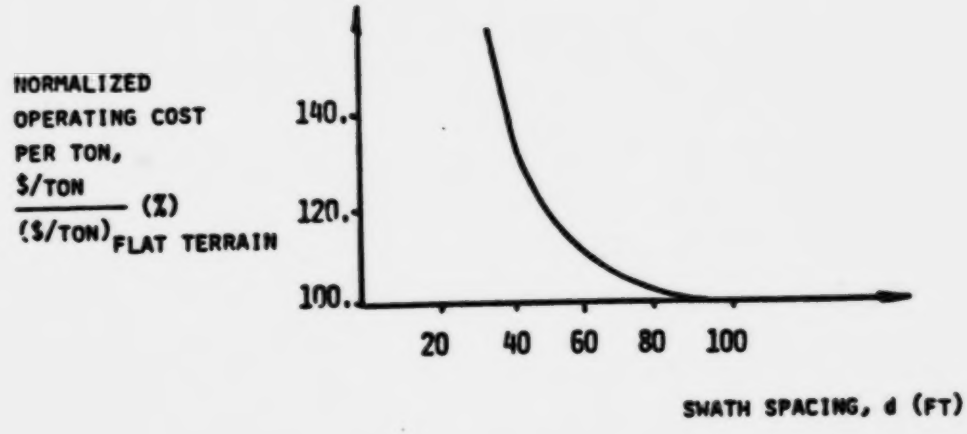

Figure 4.4. Relative Production Cost Versus Swath Spacing for Operations on a Rough Terrain

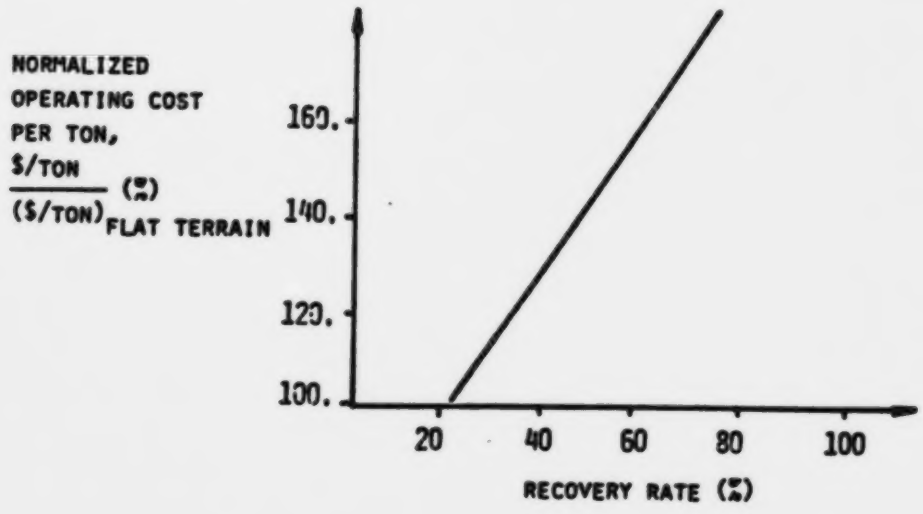

Figure 4.5. Relative Production Cost Versus Recovery Rate for Operations on a Rough Terrain

5. STUDY OF OPERATIONS WITH RESPECT TO OBSTACLES

In terms of deep ocean mining operations, an obstacle may be defined as any feature on the bottom which an ocean miner desires to avoid. For present purposes, we will consider obstacles which have been detected and mapped in a presurvey. In the following, a methodology for quantifying the effects of obstacles in terms of mine area requirements, production rate, and operating cost will be developed and illustrative examples presented.

Figure 5.1 illustrates a basic strategy for obstacle avoidance. In a region around the obstacle, successive collector swaths are compressed together and a turning maneuver is required to avoid the obstacle. An "obstacle affected area" around the obstacle may be defined. The upper and lower boundaries of the obstacle affected area are taken as the first collector swath which will be mined without reference to the presence of the obstacle and the left and right boundaries are the locus of points on the collector swaths where the collector first begins to deviate as a result of the obstacle avoidance maneuver.

The desired collector obstacle avoidance paths are as illustrated in Figure 5.1. However, since the collector is controlled by maneuvering the ship, the response of the collector to a ship maneuver must be quantified. A first approximation of the desired ship maneuver is produced by a square wave rudder and thrust input as shown in Figure 5.2. The output, collector maximum lateral motion A and lead distance D are plotted in Figures 5.2 and 5.3 for various values of thrust and maneuver period . These curves are used for determining the rudder and thrust input required to produce a desired collector maneuver output.

In reality, the collector trajectories resulting from an obstacle avoidance maneuver will not be smooth paths as illustrated in Figure 5.1, but will be subject to random lateral motion due to the various effects cited earlier. Figure 5.4 illustrates a realization of a maneuver on a random

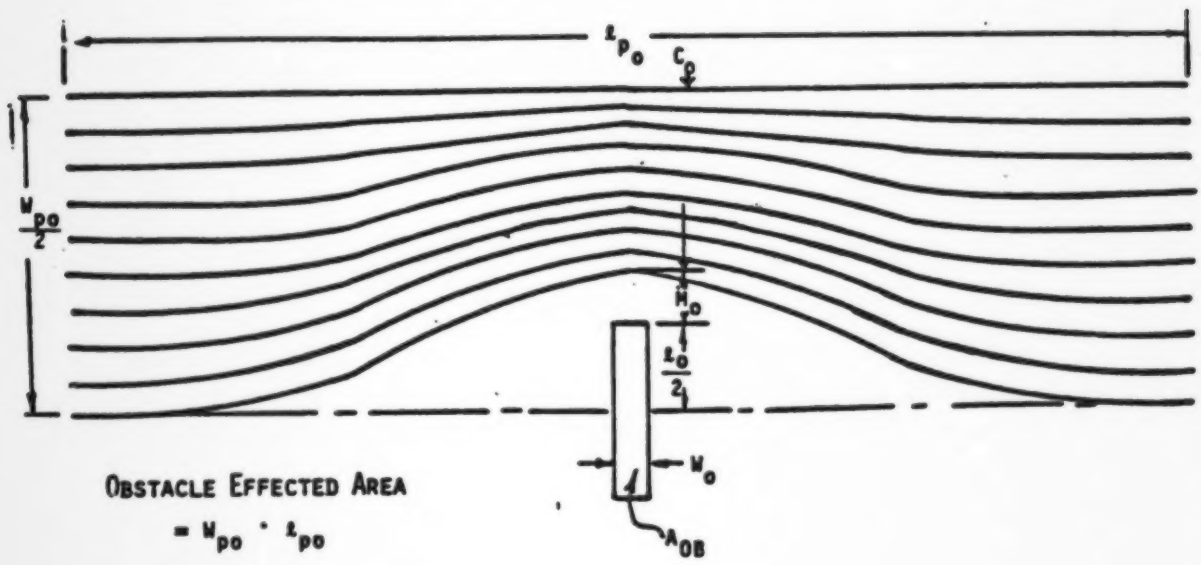

Figure 5.1. Obstacle and Obstacle Avoidance Geometry

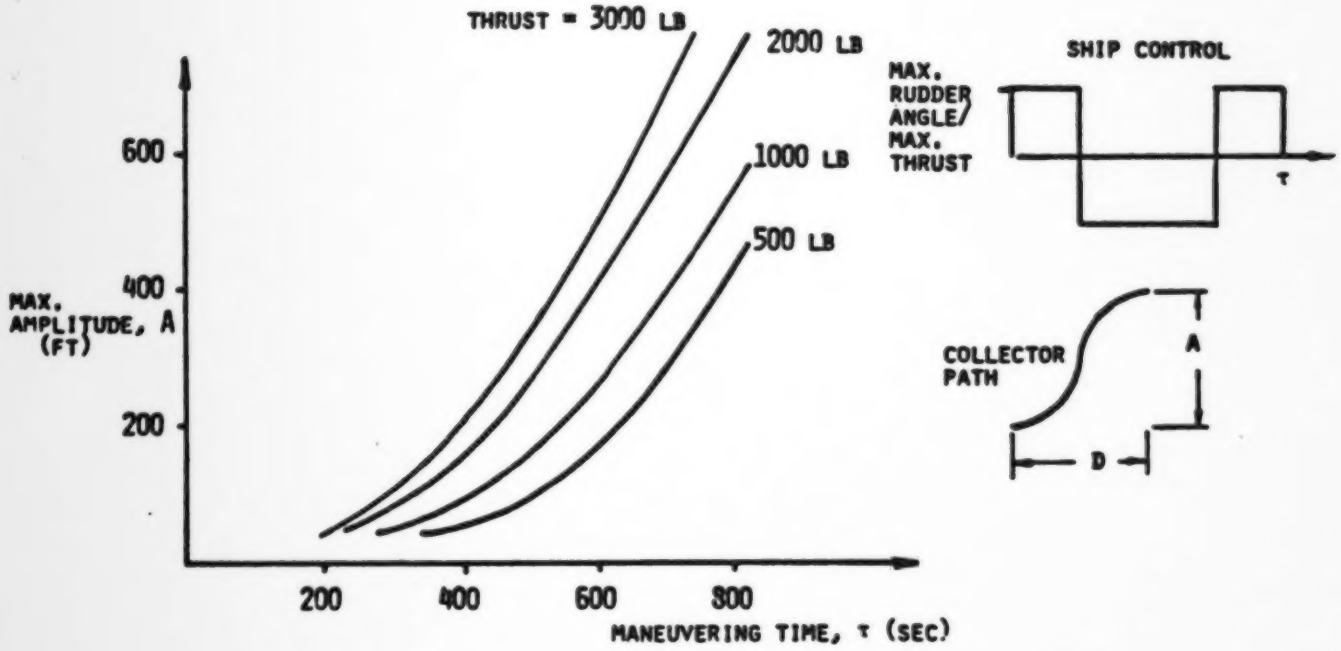

Figure 5.2. Maximum Amplitude of Collector Lateral Motion Versus Maneuver Duration for Various Values of Thrust (From Thrusters)

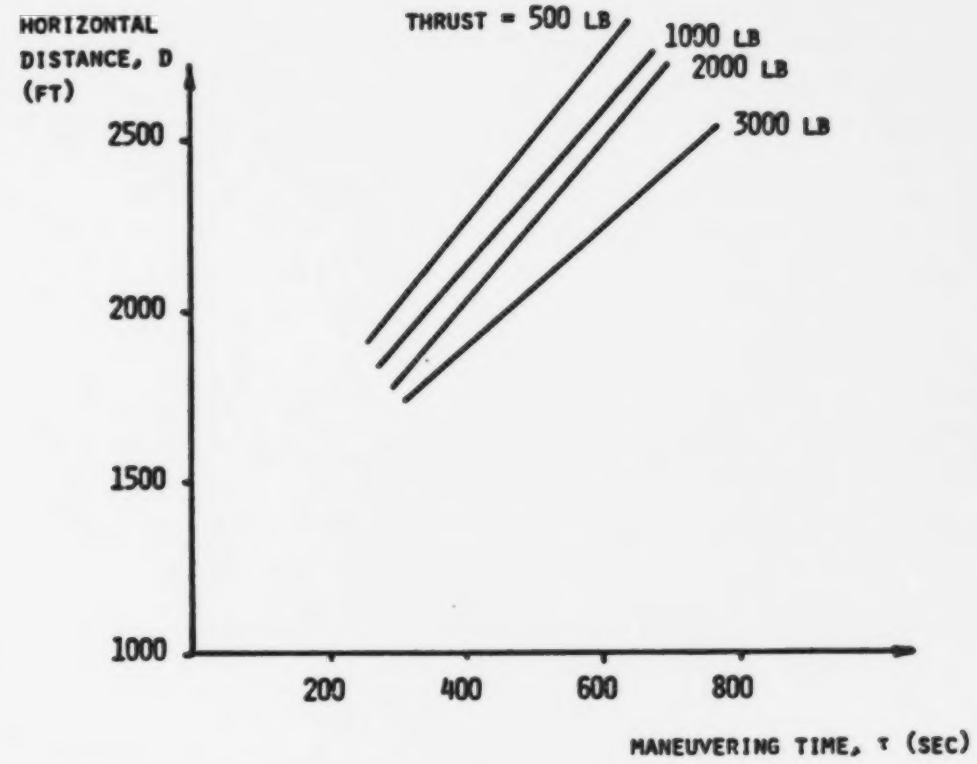

Figure 5.3. Distance D as a Function of Maneuvering Duration for Various Values of Thrust

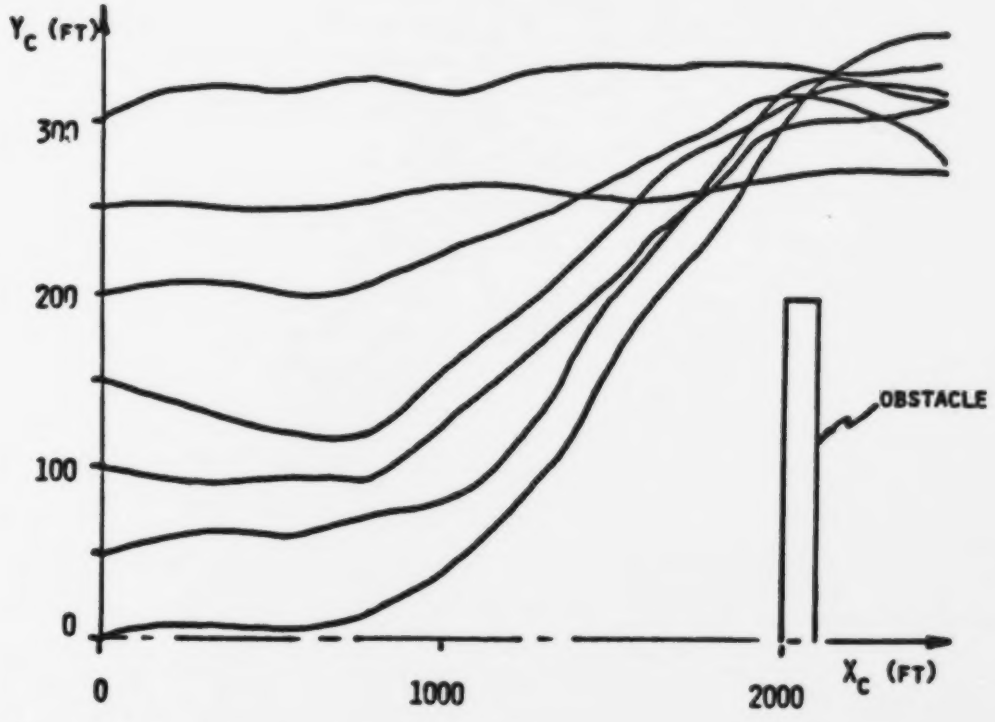

Figure 5.4. Simulated Obstacle Avoidance Trajectory of a 400 ft Obstacle

topography around a 400 ft obstacle produced by the DOMOPS. It was intended that all the swaths would go through the same point 300 ft from the center of the obstacle, that is, the compression distance C_o was zero in this case. However,as expected, this was not quite achieved because of the effect of the topography.

Figure 5.5 shows the effect of the obstacle for various collector swath widths when the swath spacing upon entering the obstacle affected area is 50 ft. The figure compares performance in the region when the obstacle avoidance maneuvers are performed with the case in which no obstacle is present. It is to be noted that the sweep efficiency shown applies to the entire obstacle affected area $W_{ob} \cdot \ell_{ob}$ and that sweep efficiency and feed efficiency are almost unaffected for large swath spacing, low recovery rate, operations.

Figure 5.1 shows that as the compression distance C_o is increased, the collector swath can be separated by greater distances at point D. Thus, an improvement in feed efficiency over the obstacle effected area would be expected. However, the obstacle affected area increases because W_o increases directly with C_o. The question is what is the net effect of varying C_o on production rate and other variables. Figure 5.6 compares the baseline case (C_o = 0, s/d = 1) to a case in which C_o has been increased, C_o = 100 ft. This figure shows a plot of cost per obstacle versus the transverse dimension of the obstacle. The cost is largely a result of lost production associated with reduced feed efficiency--a replacement cost of $36.5/DST was used for this calculation. The figure strongly suggests that the unfavorable consequences of an obstacle are minimized when C_o = 0.

Figure 5.6 also shows the consequences of decreasing the approach distance D. Costs are increased somewhat in this case, which suggests that the baseline value of D, or even a larger D may be optimum.

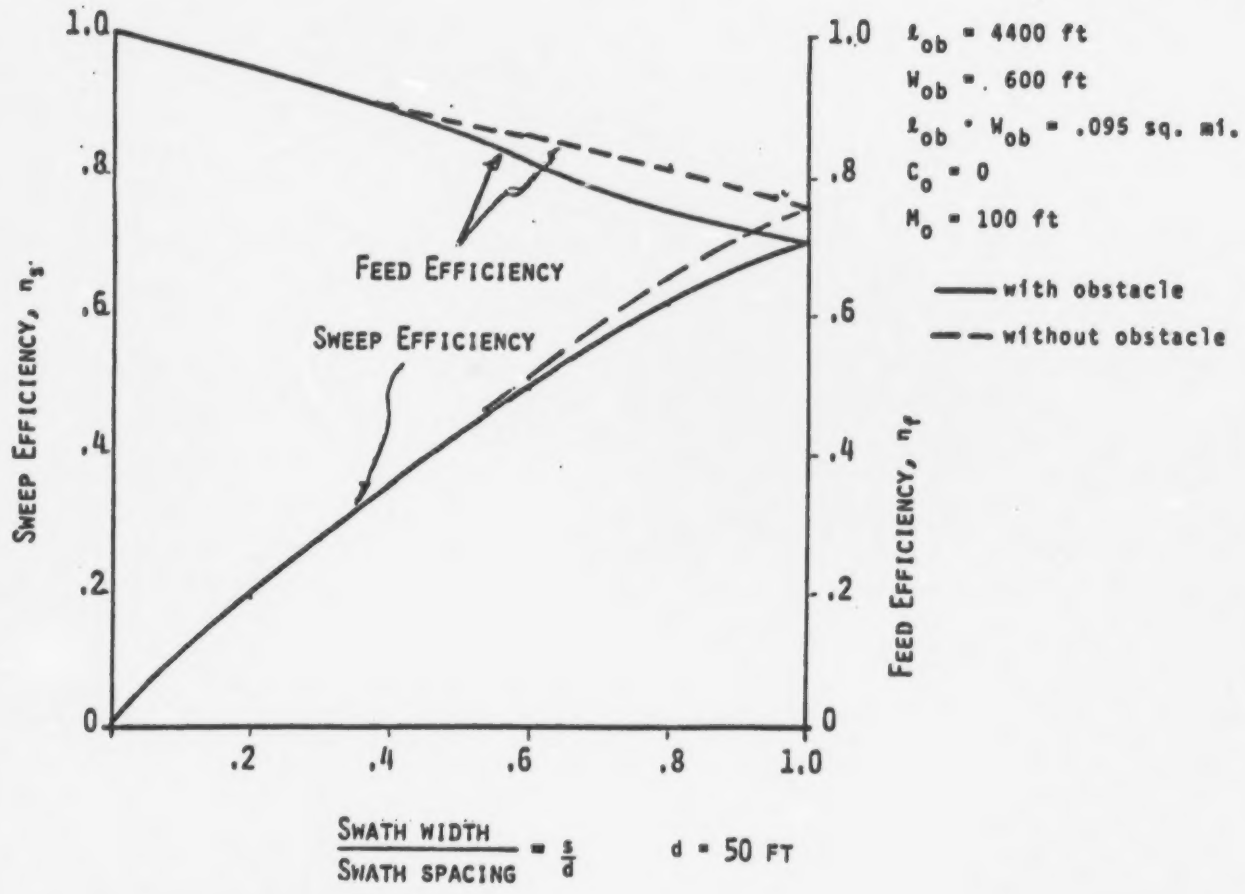

Figure 5.5. Effect of a 400 ft Obstacle on Collector Performance

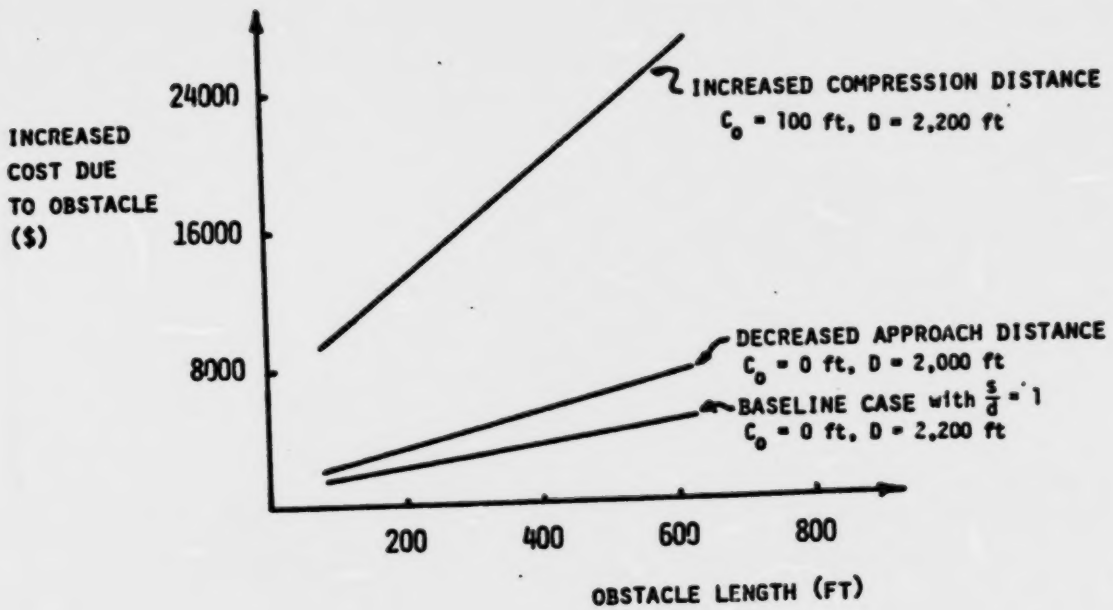

Figure 5.6. Increased Cost of Mining Due to Obstacles

6. EFFECTS OF OBSTACLES ON MINE DEVELOPMENT AND REQUIREMENTS

The results presented in the discussion of Section 5 pertain to single obstacles. It remains to establish the overall effects of obstacles on production costs, mine area requirements, and recovery rate.

Mine area requirements are defined in Flipse, Dubs, and Greenwald (1973) as

$$A_m = \frac{PL}{C\eta_d\eta_s[1-(g+a)]} \quad \frac{1}{3588} \tag{6.1}$$

where A_m = Required mine area, Km^2

P = Production rate, DSTPY

L = Mine life, years

C = Nodule concentration, wet lb/ft^2

η_d = Dredge efficiency

η_s = Sweep efficiency

g = Fraction of area below cut-off grade/concentration criterion

a = Fraction of mine unminable due to obstacles

The parameter a in Equation (6.1) defines the fraction of the mine area which is unminable due to obstacles. However, the results of this study indicate that the effect of an obstacle is not to reduce mine area at all, but that the obstacle effect is a modification of the system feed and sweep efficiencies in a region around the obstacle which we have called the "obstacle effected area." However, where there are extensive fields of obstacles, the combined area may be represented by a parameter such as a in Equation (6.1), but other obstacles which must be accommodated in the planning of collector trajectories do not contribute to a reduction in mine area. Thus, a and η_s in Equation (6.1) should be redefined as follows:

a = Fraction of mine unminable over extensive areas (not includable within subareas)

η_s = Area-weighted sweep efficiency defined by Equation (6.4)

If the area effected by obstacle i is denoted A_{obi}, then the total obstacle effected area in a mine site may be written

$$A_{ot} = \sum_i A_{obi} \tag{6.2}$$

which is the total minable area effected by obstacles.

The portion of the minable area free of obstacle effects is

$$A_m (1 - (g + a)) - A_{ot} \tag{6.3}$$

The sweep efficiency, η_s, in the denominator of Equation (6.1) must account for the sweep efficiency obtained in areas free of obstacle effects as well as obstacle effected mines. The sweep efficiency may be written

$$\eta_s = \frac{\eta_s' \ (A_m (1 - (g + a)) - A_{ot}) + \sum_i \eta_{si} A_{obi}}{A_m (1 - (g + a))} \tag{6.4}$$

where η_{si} is the sweep efficiency achieved in the obstacle effected area of obstacle i, and η_s' is the sweep efficiency in areas free of obstacle effects. The sweep efficiency, η_s, shown in Equation (6.4) is an area weighted average over the life of the mine.

Similar results may be obtained for average recovery rate and operating cost as follows:

$$R = \frac{R_m[A_m[1 - (g+a)] - A_{ot}] + \sum_i R_i A_{obi}}{A_m[1 - (g+a)]}$$

$$\overline{\$} = \frac{\$_m R_m [A_m [1 - (g+a)] - A_{ot}] + \sum_i R_i \$_i A_{obi}}{A_m R [1 - (g+a)]} \tag{6.5}$$

Equations (6.4) and (6.5) may be applied in two ways: (1) if all of the obstacles in a mine site have been surveyed, the areas A_{obi} and other parameters can be estimated for each obstacle and the results summed as indicated in the equations; and (2) if the lengths, orientations, and spatial density of obstacles in minable areas can be described statistically, the statistics of the quantities in Equations (6.4) and (6.5) could be derived. Presently, the second of these two methods is the more feasible of the two. It is suggested that this be considered in a subsequent effort.

7. FORMULATION OF THE DOMOPS CAPABILITY

Section 2 describes the overall approach and requirements on which the DOMOPS capability is to be based. Figure 2.2 shows the global (XYZ) coordinate system, the position of the collector (X_c, Y_c, Z_c) in this coordinate system and the position of the ship CG (X_s, Y_s, Z_s) in this global coordinate system.

The lift pipe generally assumes a cantenary shape. It will be assumed in the formulation development that the relative vertical displacement of the ship and collector does not alter the catenary shape. Thus, in this case, the two-dimensonal coordinate system X,Y shown in Figure 7.1 will be used.

Figure 7.1 also defines a collector-bound (x,y) coordinate system. The origin of the (x,y) coordinate system is located at the collector CG with the x-axis in the direction of the collector velocity. Figure 7.1 also shows the ship-bound coordinate system (x_1, y_1), which is defined with its origin at the ship CG, with the x_1 axis along the longitudinal axis of the ship, pointed toward the bow. The y_1-axis is positive to port. The angle Θ_s defines the ship heading, and β_s is the drift angle.

Equations of Collector Motion

The collector motion is described by two degrees of freedom in the horizontal plane, X_c and Y_c. The Newtonian equations of motion for the collector are,

$$F_{cX} = m_{cXX}\ddot{X}_c + m_{cXY}\ddot{Y}_c$$
$$F_{cY} = m_{cYX}\ddot{X}_c + m_{cYY}\ddot{Y}_c \qquad (7.1)$$

where F_{cX} and F_{cY} are the net forces on the collector in the X and Y directions, respectively. $\ddot{X}_c$ and $\ddot{Y}_c$ are the collector accelerations in the global coordinate system. Because of the hydrodynamic phenomenon of added mass, the collector virtual masses, m_{cXX} and m_{cYY}, are not identical and the coupling term, m_{cXY}, exists. They may be obtained in terms of the collector surge and sway virtual mass, m_{cs} and m_{cy}, and the collector heading angle, θ_c, as

$$\begin{aligned} m_{cXX} &= m_{cx} \cos^2 \theta_c + m_{cy} \sin^2 \theta_c \\ m_{cXY} &= (m_{cx} - m_{cy}) \sin \theta_c \cos \theta_c \\ m_{cYY} &= m_{cx} \sin^2 \theta_c + m_{cy} \cos^2 \theta_c. \end{aligned} \tag{7.2}$$

The equations of motion, Equation (7.1), may be solved simultaneously to obtain the collector acceleration in the global coordinate system,

$$\begin{aligned} \ddot{X}_c &= \frac{m_{cYY} F_{cX} - m_{cXY} F_{cY}}{m_{cXX} m_{cYY} - m_{cXY}^2} \\ \ddot{Y}_c &= \frac{m_{cXX} F_{cY} - m_{cXY} F_{cX}}{m_{cXX} m_{cYY} - m_{cXY}^2} \end{aligned} \tag{7.3}$$

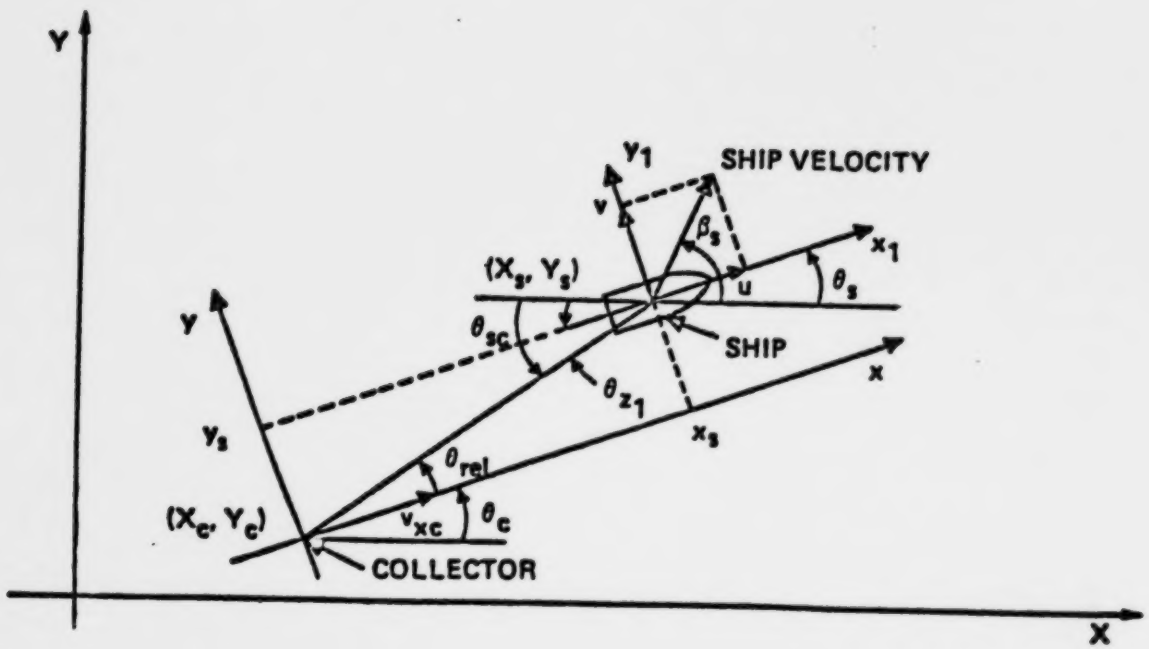

Figure 7.1. Coordinate System Definitions

Collector Forces

The collector is acted upon by four forces:

1. Gravity
2. Sediment Drag
3. Hydrodynamic Drag
4. Lift String Forces

Let the sediment profile be described by the function h(X,Y). The gravity force tends to cause the collector to slide downhill, and for small slope angles, is proportional to the sediment slope:

$$F_{gX} = - W \frac{\partial h(X_c, Y_c)}{\partial X}$$

$$F_{gY} = - W \frac{\partial h(X_c, Y_c)}{\partial Y} \qquad (7.4)$$

where W is the collector weight in water.

The sediment drag force will be assumed in the form of coulomb friction, and thus acts as a constant force opposite to the direction of motion. Therefore, constant force longitudinally:

$$F_{dx} = - \mu W \frac{v_{cx}}{|v_{cx}|} \qquad (7.5)$$

where μ is the sediment coefficient of friction, and v_{cx} is the collector velocity because the x axis is defined to be coincident with the collector

velocity vector. Thus, collector transverse velocity, $v_{cy} = 0$, and there is no force component in the transverse direction due to sediment drag.

The hydrodynamic drag force on the collector is proportional to the square of velocity. Therefore,

$$F_{hx} = - C_D A_x \frac{1}{2} \rho v_{cx}^2 \tag{7.6}$$

where C_D is the collector surge drag coefficient, A_x is the transverse area, and X is the density of sea water.

The lift pipe force is much more complicated. The derivation in Appendix B shows how a simple model was developed for the lift pipe, resulting in these expressions for the lift pipe force:

$$F_{\ell x} = K_x x_s$$

$$F_{\ell y} = K_y y_s - b_y v_{cx} \sin \theta_{rel} \tag{7.7}$$

Transforming the forces in the collector-bound coordinate system gives the forces on the collector in the global coordinate system,

$$F_X = F_x \cos \theta - F_y \sin \theta$$

$$F_Y = F_x \sin \theta + F_y \cos \theta$$

Combining the transformed forces and the gravity force which was originally computed in global coordinates gives the net force on the collector in the global coordinate system, which may be substituted into Equations (7.3) to determine the collector motion.

Ship Equations of Motion

The motion of the ship is described in Figure 7.1 by three degrees of freedom, X_s, Y_s and X_s. The development of the Newtonian equations of motion for the ship follows exactly that of the collector with the addition of the variable X_s representing the ship heading, and are

$$\ddot{X}_s = \frac{m_{sYY} F_{sX} - m_{sXY} F_{sY}}{m_{sXX} m_{sYY} - m_{sXY}^2}$$

$$\ddot{Y}_s = \frac{m_{sXX} F_{sY} - m_{sXY} F_{sX}}{m_{sXX} m_{sYY} - m_{sXY}^2}$$

$$\ddot{\theta}_s = \frac{M_{sZ}}{I_{sZ}} \qquad (7.8)$$

where the ship mass terms are calculated as in Equation (7.2) by substituting the s subscript for the c. M_{sZ} is the net moment on the ship about the vertical axis, and I_{sZ} is the moment of inertia of the ship about the same axis.

Ship Forces

The forces acting on the ship are of two types: environmental forces, which are determined by nature, and control forces, which are controllable within the limitations of propulsion system and maneuvering system design.

Environmental Forces

The environmental forces acting on the ship considered in this study are those due to:

1. Lift pipe drag
2. Wave drift forces
3. Wind force
4. Frictional and form resistance of the hull.

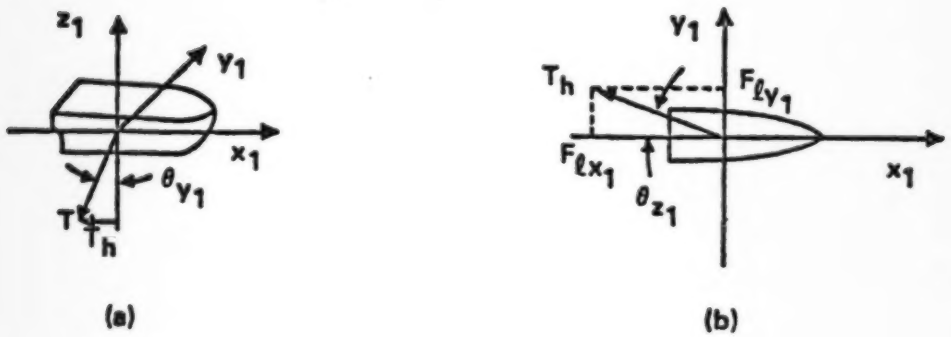

Figure 7.2. Components of lift pipe tension

It is assumed that changes in force on the ship result from changes in the direction of the tension. Referring to Figure 7.3, if we assume that a straight line between the ship and collector defines the nominal direction, then deviations in the ship's path from this line will result in a transverse force on the ship. The angle of the line between the collector and the ship is called θ_{sc} and the heading of the ship is θ_s, both in the global coordinate system, then the relative angle of the lift pipe is,

$$\theta_{z_1} = \theta_s - \theta_{sc} \tag{7.9}$$

Then, since from Figure 7.2, the horizontal component of the lift pipe tension is

$$T_h = T \sin \theta_{y_1} \tag{7.10}$$

the lift pipe drag forces and moment are,

$$\begin{aligned} F_{\ell x_1} &= - T_h \cos \theta_{z_1} \\ F_{\ell y_1} &= - T_h \sin \theta_{z_1} \\ M_{\ell z_1} &= F_{\ell y_1} x_{\ell s} \end{aligned} \tag{7.11}$$

where $x_{\ell s}$ is the distance from the ship CG to the lift string attachment point, in the ship-bound coordinate system.

Reference 1 gives the steady environment loads on the ship due to wind, wave drift forces, and hull resistance. These loads are summarized here.

Let the heading of the relative wind be defined by α_{wr}, as shown in Figure 7.3.

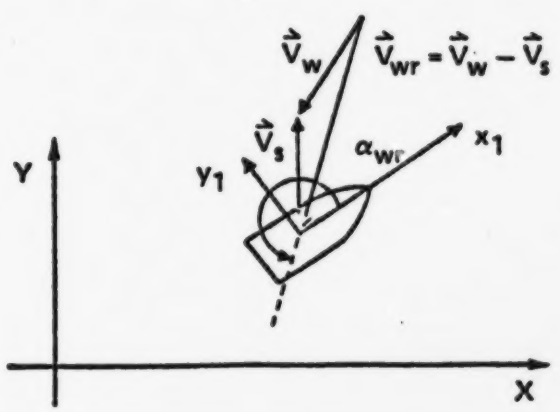

Figure 7.3. Definition of Relative Heading

The wind loads in terms of the dynamic pressure and measured parameters are,

$$F_{wx_1} = C_{wx_1}(\alpha_{wr})\, A_t\, q_w$$

$$F_{wy_1} = C_{wy_1}(\alpha_{wr})\, A_\ell\, q_w$$

$$M_{wz_1} = C_{wz_1}(\alpha_{wr})\, A_\ell\, L\, q_w \qquad (7.12)$$

where F_{wx_1} is the steady surge wind force, F_{wy_1} is the steady sway wind force, and M_{wz_1} is the steady wind yaw moment. A_t is the ship transverse area, A_ℓ is the ship longitudinal area, L is the ship length, and C_{wx_1}, C_{wy_1}, and C_{wz_1} are empirical force and moment coefficients defined in Reference 1.

Let V_{wr} define the relative speed between the ship and the wind. Then the dynamic pressure of the wind, q_w, is given by,

$$q_w = \frac{1}{2}\rho_a V_{wr}^2 \qquad (7.13)$$

where ρ_a is the mass density of air.

The steady hull resistance loads are calculated in an identical manner to the wind loads by substituting the subscript c for the subscript w, with one exception. For flow in the longitudinal direction, the ship is a slender body, and at towing speeds, the resistance is primarily due to skin friction. The frictional resistance is approximately given by the formulas for a flat plate, in terms of the ship forward velocity, u, as

$$F_{cx_1} = \frac{.075}{(\log Re_\ell - 2)^2} \cdot \frac{1}{2} \rho u^2 \cdot S \tag{7.14}$$

where S is the wetted surface area and Re_ℓ is the Reynolds's number based on ship length given by

$$Re_\ell = \frac{uL}{\nu} \tag{7.15}$$

where L is ship length and ν is the kinematic viscosity of sea water.

The longitudinal drift force as well as the drift moment is assumed negligible. Reference 1 gives the mean lateral drift force in irregular waves as,

$$F_{fy_1} = \rho g L \sin^2 \alpha_{wr} \int_0^\infty R^2 \, S(\omega) \, d\omega \tag{7.16}$$

where g is the acceleration of gravity, $S(\omega)$ is the sea power spectral density, and $R(\omega)$ is the non-dimensional drift force response in regular waves, given in Reference 1.

Control Forces

Three systems are available to the simulation operator for maneuvering. These are the main propulsion system, the thrusters (one forward and one aft), and the ship's rudder. Each maneuvering system is subject to the contol logic of Figure 7.4.

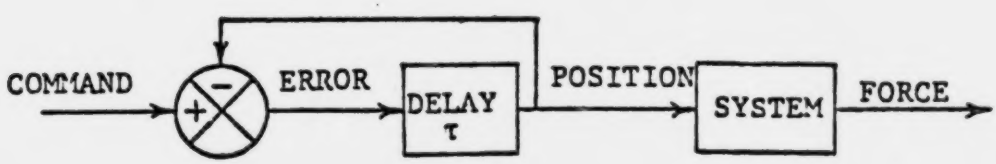

Figure 7.4. Maneuvering System Control Logic

During the simlation, each maneuvering system may be issued a control command as a function of time. The command is compared to the current position and the error computed. The error is subject to a first-order time delay before describing the new position. The new position then acts through the system to create maneuvering forces. Reference 2 describes the hydrodynamic forces on the rudder in terms of an empirical lift coefficient, D_{L_R}, and drag coefficient, C_{D_R}, as shown in Figure 7.5.

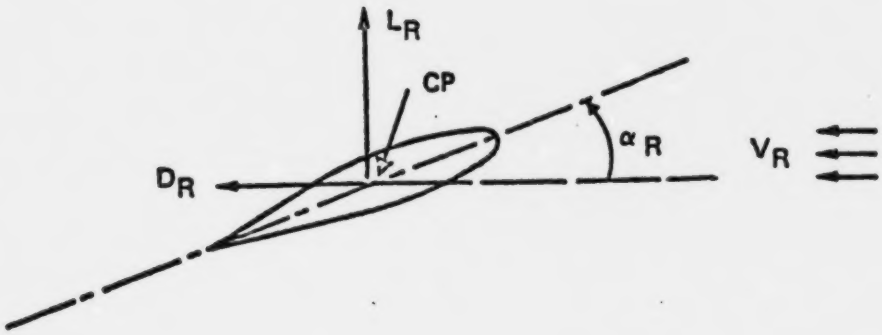

Figure 7.5. Rudder Hydrodynamic Forces

Thus,

$$L_R = C_{L_R}(\alpha_R)\, A_{T_R}\, \tfrac{1}{2}\, \rho\, V_R^2 \tag{7.17}$$

$$D_R = C_{D_R}(\alpha_R)\, A_{T_R}\, \tfrac{1}{2}\, \rho\, V_R^2 \tag{7.18}$$

where L_R is the lift force on the rudder, D_R is the drag force on the rudder, α_R is the angle of attack of the rudder, and V_R is the rudder velocity relative to the ambient flow.

Because the ship may be translating and rotating, the geometric velocity at the rudder may be different from that at the CG of the ship. The actual drift angle at the rudder is called β_R, which is shown in Figure 7.6. In terms of β_R, the rudder force and moment on the ship are,

$$F_{Rx_1} = L_R \sin \beta_R - D_R \cos \beta_R$$

$$F_{Ry_1} = L_R \cos \beta_R + D_R \sin \beta_R$$

$$M_{Rz_1} = F_{Ry_1} \cdot x_R \tag{7.19}$$

Note that D_R is always positive in the direction of flow, and x_R is negative for a stern-mounted rudder.

The ship propulsion system is assumed to consist of a pair of diesel prime movers whose total brake horsepower output is P_B, and fuel consumption per horsepower rate is $\dot{r}_p$. The diesel prime movers drive the propeller shaft through a set of reduction gears and the propeller shaft which is seated in a tunnel bearing.

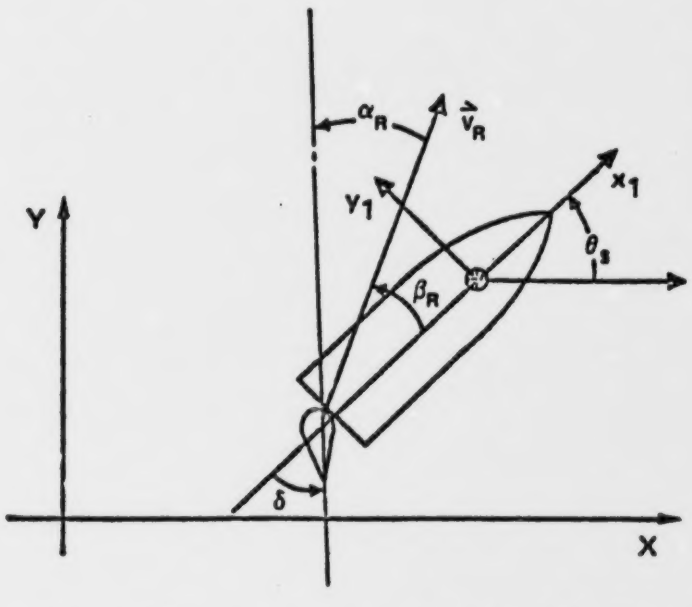

Figure 7.6. Definition of Rudder Velocity

The associated efficiencies are η_T, η_S, and η_D, respectively. The propeller efficiency, η_E, is given by

$$\eta_E = \eta_H \cdot \eta_R \cdot \eta_O \tag{7.20}$$

where η_H is the hull efficiency, η_R is the relative rotative efficiencu, and η_0 is the open-water propeller efficiency. The propulsion efficiency is then

$$\eta_P = \eta_E \cdot \eta_T \cdot \eta_S \cdot \eta_D \tag{7.21}$$

and the propulsion power is then

$$P_P = \eta_P P_B. \tag{7.22}$$

The propulsion force from the main propeller is then,

$$F_{Px_1} = \frac{P_P}{u} \tag{7.23}$$

and the fuel consumption is

$$f_{cp} = \int_o^t \dot{r}_P \cdot P_B \, dt \tag{7.24}$$

The thruster forces and fuel consumption are calculated in a similar manner, except that a single figure characterizes each thruster force:

$$F_{ty_1} = f_t \cdot P_t$$

$$M_{tz_1} = F_{ty_1} \cdot x_t, \tag{7.25}$$

where P_t is the commanded thruster power, f_t is the thruster thrust/power ratio, and x_t is the distance from the ship CG to the thruster along the x_1 axis. The thruster fuel consumption is calculated from

$$fc_t = \int_0^t \dot{r}_t \cdot P_t \, dt \tag{7.26}$$

This completes the simulation development, except for the sweep efficiency calculation which is in the process of development. The collector and ship equations of motion, represented by Equations (7.3) and (7.8) respectively, were solved using a fourth-order Runge-Kutta numerical integration routine. The entire simulation is computerized, allowing simulation of a wide range of deep ocean mining system configurations in a convenient manner.

8. CONCLUSIONS AND RECOMMENDATIONS

These initial investigations were based upon utilization of the DOMOPS capability. The DOMOPS program is an efficient tool (23 cents per mile) for analyzing deep ocean mining operations, including:

- Obstacles
- Rough terrain
- Weather
- Mining system design parameters
- Operational parameters

In addition, several general conclusions can be stated:

- Rough terrain decreases both sweep efficiency and feed efficiency of nodule collection

- Collector maneuverability from the surface is greatly limited by the length of the lift pipe and the drag of seawater

- Increasing forward velocity of the collector increases sensitivity to side slopes

- Lift pipe drag has a significant effect on mining ship maneuverability

The presence of obstacles further reduces sweep efficiency and feed efficiency. However, this reduction is minimal for a system whose sweep efficiency is low to begin with. Other conclusions regarding obstacle effects are as follows:

- The effect of an obstacle may be viewed as occurring over an obstacle effected area in which feed and sweep efficiency are modified. The overall effects on the mine site are thus obtained by combining the

sweep efficiency and feed efficiency for obstacle and nonobstacle areas on an area weighted basis.

- Effects of obstacles are sensitive to the controllability of the collector. The results presented account for the effects of rough terrain. Other effects such as navigational error, wave drift forces, temporal and spatial current variations will further degrade performance with respect to obstacles and in general. However, these effects can be countered by using collector steering.

- Using the same miss distance for all obstacle paths minimizes obstacle avoidance operating cost, cost of lost production, and also maximizes mine site recovery rate.

- Overall assessment of obstacle effects on mine area, recovery rate, and average production rate requires utilization of information on obstacle size distribution and spatial density.

9. REFERENCES

1. Remery and Van Oortmerssen, "The Mean Wave, Wind, and Current Forces on Offshore Structures and Their Role in the Design of Mooring Systems," OTC 1741, 1973.

2. Comstock, J. P. (ed.), Principles of Naval Architecture, Society of Naval Architects and Marine Engineers, New York, 1977.

3. Woodson, H. H., and Melcher, J. R., Electromechanical Dynamics, John Wiley Sons, New York, 1968, p. 577 ff.

APPENDIX A. NOMENCLATURE

A = coefficient defined by Equation (B.5)

A_T = transverse area

B = coefficient defined by Equation (B.6)

b_c = linearized collector damping coefficient

b_x = lift pipe damping coefficient per unit length

b_y = lumped damping coefficient

C = empirical coefficient defined in Reference 1

C_D = drag coefficient

C_L = lift coefficient

D = lift pipe diameter

D_R = rudder drag force

F = force

f_t = thruster specific thrust

fc = fuel consumption

h = sediment height

I_s = ship virtual moment of inertia

K = lift pipe spring constant

L = ship length

L_R = rudder lift force

M = moment

m = mass

P_B = brake horsepower

P_p = propulsion power

q = dynamic pressure

R = non-dimensional drift force coefficient, lift pipe radius of curvature

$\dot{r}_p$ = main propulsion system specific fuel consumption

$\dot{r}_t$ = thruster specific fuel consumption

Re_ℓ = Reynold's number based on ship length

S = wetted surface area

T = maximum lift pipe tension

t = time

T_o = average lift pipe tension

u = ship surge velocity

V = velocity

v = ship sway velocity

W = collector weight in water

x_R = distance from rudder CP to ship CG

x_t = distance from thruster to ship CG

X,Y,Z = global coordinate system

x,y = collector-bound coordinate system

x_1,y_1 = ship-bound coordinate system

x',y',z' = lift pipe coordinate system

α = angle of attack

β = drift angle

δ = rudder angle

η_D = bearing efficiency

η_E = propeller efficiency

η_H = hull efficiency

η_O = propeller open-water efficiency

η_P = propulsion efficiency

η_R = propeller relative rotative efficiency

η_S = shaft efficiency

η_T = transmission efficiency

Θ = angular displacement

Θ_{rel} = angular displacement defined in Figure 3.1

μ = sediment coefficient of friction

ρ = sea water density

ρ_a = air density

ω_d = driving frequency

Subscripts

c = collector, current

d = sediment drag

f = wave drift force

g = gravity

h = hydrodynamic drag, horizontal

ℓ = lift pipe

P = main propulsion

R = rudder

s = ship

w = wind

X,Y,Z = components of global coordinate system

x,y,z = components of collector-bound coordinate system

x_1,y_1,z_1 = components of ship-bound coordinate system

APPENDIX B. DEVELOPMENT OF A SIMPLE MODEL FOR LIFT PIPE BEHAVIOR

To determine the collector response to arbitrary ship motions, consider the motion of the ship and collector in calm seas over a flat terrain in a coordinate system x', y', z', whose origin is at the collector, and which is moving at the steady ship speed, where the coordinate x' represents the distance along the lift string. The fact that the lift pipe is curved is not significant for the purposes of this analysis as long as

$$\frac{R}{D} \gg 1$$

where R is the radius of curvature, and D is the lift pipe diameter.

The model shown in Figure B.1 then represents the lift pipe/collector system.

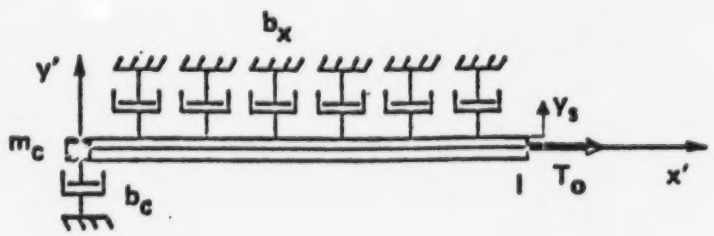

Figure B.1. Model of Lift Pipe/Collector System

where m_c is the transverse collector mass, b_c, is a linearized collector damping coefficient, T_o is the average lift pipe tension, b_x is the linearized damping coefficient per unit length due to the sea water, y_s is the transverse ship motion, and X is the length of the lift pipe. The equation for the system of Figure B.1 is (see Reference 3),

$$b_x \frac{\partial y'}{\partial t} - T_o \frac{\partial^2 y'}{\partial x'^2} = 0 \tag{B.1}$$

with the boundary conditions,

$$y'(\ell, t) = y'_s(t) \tag{B.2}$$

$$T_o \frac{\partial y'(0, t)}{\partial x} = + m_c \frac{\partial^2 y'}{\partial t^2} + b_c \frac{\partial y'}{\partial t} \tag{B.3}$$

Equation B.1 is an example of the diffusion equation for which the sinusoidal steady-state solution is

$$y' = (Ae^{-ikx} + Be^{ikx}) e^{i\omega_d t} \tag{B.4}$$

where A and B are determined by the boundary conditions (B.2) and (B.3) which yield,

$$A = \frac{-\left[-m_c\omega_d + i(v_c\omega_d - T_oK)\right]}{\left[-m_c\omega_d + i(b_c\omega_d + T_oK_d)\right] e^{ik\ell} - \left[-m_c\omega_d + i(b_c\omega_d - T_ok)\right] e^{-ik\ell}} \tag{B.5}$$

$$B = \frac{1 - Ae^{-k\ell}}{e^{ik\ell}} \tag{B.6}$$

The desired response is then

$$\frac{y'(0)}{y'(\ell)} = A + B \tag{B.7}$$

where A and B are given above.

The system shown in Figure B.1 can also be modeled with the simple system shown below.

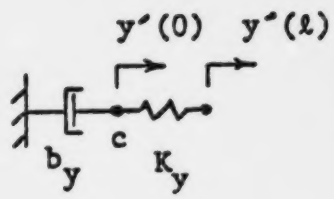

Figure B.2. Simple Model of the Lift Pipe

The equation of motion for the system of Figure B.2 is

$$m_c\ddot{y}'(0) + b_y y'(0) + K_y y'(0) = K_y y'(\ell) \tag{B.8}$$

The sinusoidal steady state response to Equation B.8 is

$$\frac{y'(0)}{y'(\ell)} = \frac{K_y}{i\omega_d b_y + K_y - m_c\omega_d^2} \tag{B.9}$$

Therefore, the objective is to choose the optimum values of K_y, b_y such that Equation (7.5) and Equation (7.7) are nearly identical over the frequency range of interest. Note that the two equations are automatically equal at $\omega_d=0$. This resulted from a judicious choice of model shown in Figure B.2. The value of b_y is determined by matching Equation (7.7) with Equation (7.5) at a single frequency. Since the equations match at $\omega=0$, it is natural to choose b_y so that the equations are also matched at the highest frequency of interest, $\omega=\omega_{max}$. A computer program was written to perform this task automatically. Figure B.3 shows how well the frequency response matches over the entire range of frequencies $0\leq\omega_d\leq\omega_{max}$. Therefore the simple system of Figure B.2 provides an excellent model for the collector response to ship motions.

The transverse lift string force is therefore the force on point c of the simple system of Figure B.2 which is

$$F_{\ell_y} = K_y\, y'(0) - y'(\ell) \;- b_y \dot{y}'(\ell) \tag{B.10}$$

This becomes, in the coordinate system used in the main body of the report,

$$F_{\ell_y} = K_y y_s - b_y v_{cx} \sin \theta_{rel}$$

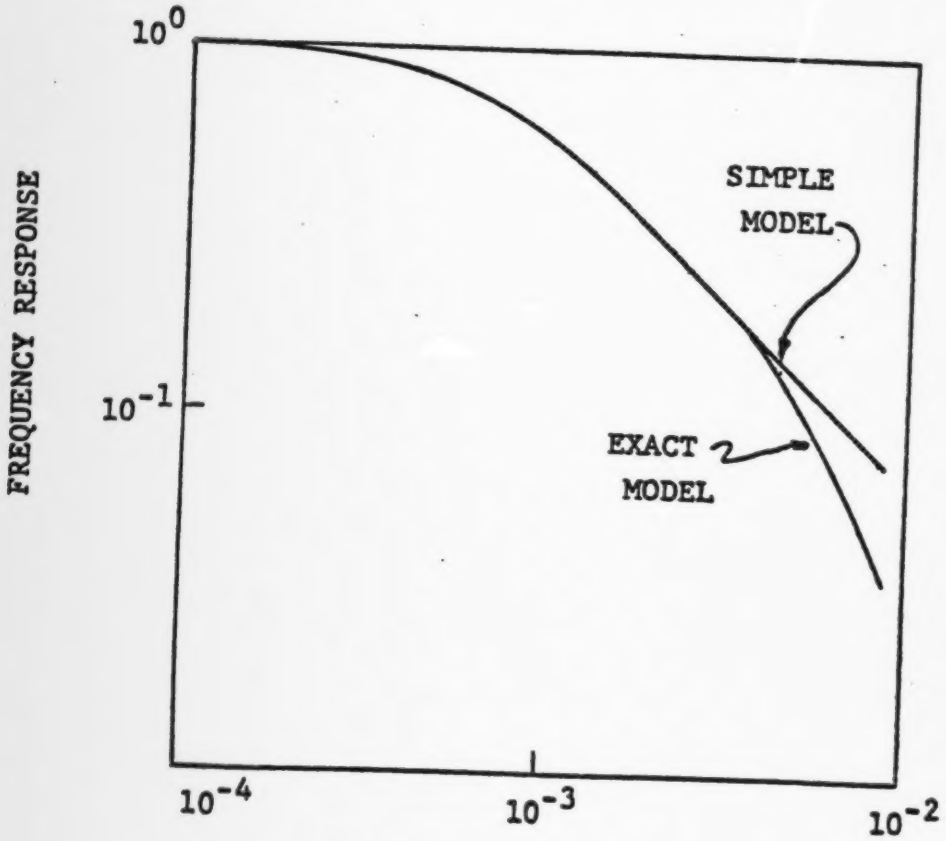

Figure B.3. Comparison of Frequency Response of Simple Model to That of Exact Model